Materials Science & Engineering A 579 (2013) 157–163

Contents lists available at SciVerse ScienceDirect

Materials Science & Engineering A

journal homepage: www.elsevier.com/locate/msea

Influence of stress field of expanding and contracting plate shaped precipitate on hydride embrittlement of Zr-alloys

R.N. Singh [a,b,c,*], H.K. Khandelwal [a,b], A.K. Bind [a,b], S. Sunil [a,b], P. Ståhle [c,d]

[a] Mechanical Metallurgy Division, Bhabha Atomic Research Centre, Mumbai 400085, India
[b] Homi Bhabha National Institute, Mumbai 400094, India
[c] Materials Science, Technology and Society, Malmö Högskola, SE-20506, Sweden
[d] Division of Solid Mechanics, Lund University, SE-22100, Sweden

ARTICLE INFO

Article history:
Received 21 December 2012
Received in revised form
20 April 2013
Accepted 29 April 2013
Available online 17 May 2013

Keywords:
Zr-alloy
Hydride embrittlement
Fracture toughness
Stress-field
Fully constrained

ABSTRACT

The stress fields of expanding (precipitation) and contracting (dissolution) hydride plates were computed by finite element method using Zr–H solid solution and hydride properties at 25, 200 and 400 °C for fully and semi-constrained hydride plates. For the first time simultaneous hydride expansion and matrix contraction and vice-versa have been considered in a simulation of hydride precipitation and dissolution, respectively. It was observed that a fully constrained expanding hydride plate exerts a tensile stress field in the matrix close to the edge of the hydride plate while a partially contracting hydride plate exerts a tensile stress field in the hydride plate as well as a large compressive stress in the surrounding matrix close to the edge of the hydride plate. It is suggested that a compressive stress component in the matrix acting normal to a partially shrinking hydride plate could possibly explain an enhanced resistance to hydride embrittlement of Zr-alloy at elevated temperature.

1. Introduction

Dilute zirconium alloys, by virtue of its very low neutron absorption cross-section, good corrosion resistance in aqueous medium and adequate strength, are being extensively used as in core structural components in Pressurized Heavy Water Reactor (PHWR) [1–3]. A part of the hydrogen/deuterium evolved during service from coolant–metal corrosion reaction is picked up by the components [4,5] and if present in excess of terminal solid solubility (TSS) [6,7] can precipitate out as hydride phase. Being brittle, the presence of substantial quantities of hydrides can cause embrittlement of the host matrix resulting in loss of ductility, impact and fracture toughness.

Both impact and fracture toughness of this alloy shows strong influence of hydrides below 150 °C [8,9]. As is evident from Fig. 1 (a) and (b), above 150 °C, the influence of hydrides on impact [8] and fracture toughness [9] is insignificant.

With increase in temperature, matrix ductility, solid solubility of hydrogen in matrix and the toughness of hydride are expected to increase. This could possibly explain the reduced susceptibility of this alloy to hydride embrittlement at higher temperature. However, it may be noted that the gross tensile ductility of this alloy is practically unaffected by temperature up to 300 °C [10] and hydride of this alloy reportedly fails in brittle manner up to 400 °C [11]. The increase in temperature will result in partial dissolution of hydrides, and hence the degree of hydride embrittlement (HE) can be expected to reduce in proportion to reduction in hydride volume fraction with increase in temperature. However, even though TSS of hydrogen in dilute Zr-alloys at 150 °C is about ~7 wppm only during heating [6,7], alloys containing few hundreds wppm of hydrogen are also immune to HE above 150 °C. Hence weak temperature dependence of matrix ductility and hydride toughness and reduction in hydride volume fraction with increase in temperature cannot explain the restoration of toughness of this alloy above 150 °C.

Usually, the test temperatures for carrying out elevated temperature impact and fracture toughness tests [8,9,12–16] are attained by heating the samples from ambient temperature to the test temperature. The stress field of hydride is expected to depend on whether hydride is expanding (as happens during cooling) or contracting (as happens during heating) [17]. The stress field of hydride in conjunction with externally applied stress field is expected to govern the susceptibility of hydride forming metals and alloys to hydride embrittlement. The objective of this work was to compute the stress fields of growing and contracting hydride plates so as to understand the role of direction of approach of test temperature on impact and fracture behaviour of hydride forming metals in general and Zr-alloys in particular.

2. Mechanism of transformation of α-Zr to δ-hydride

Transformation of α-Zr to δ-hydride is associated with about 17% increase in volume. Stress free transformation strain of δ-

* Corresponding author at: Mechanical Metallurgy Division, Bhabha Atomic Research Centre, Mumbai 400085, India. Tel.: +91 22 25593817; fax: +91 22 25505151.
E-mail addresses: rnsingh@barc.gov.in, rnbedeshi@gmail.com (R.N. Singh).

0921-5093/$ - see front matter © 2013 Elsevier B.V. All rights reserved.
http://dx.doi.org/10.1016/j.msea.2013.04.117

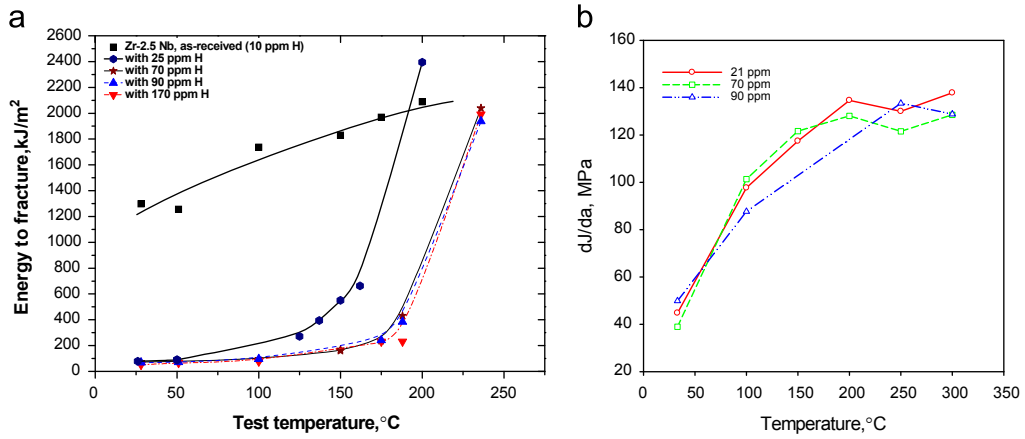

Fig. 1. Toughness of Zr–2.5 Nb pressure tube material as a function of test temperature measured as (a) total absorbed energy during impact tests [8] and (b) *dJ/da* [9].

hydride plate with respect to α-Zr from the lattice parameters of respective phases, was computed by Carpenter [18]. At ambient temperature, the in-plate transformation strain was reported to be 4.58%, while the same normal to hydride plate was 7.2%. Subsequently using Carpenter's methodology [18], Singh et al. [19] computed the temperature dependence of stress free transformation strains of δ-hydride plate with respect to α-Zr, which was reported to increase with increase in temperature. Leitch and Puls [20] attempted to understand the hysteresis associated with terminal solid solubility of hydrogen in Zr-alloys using the accommodation energy of hydrides in zirconium computed by continuum based finite element method. The transformation of hydride from matrix was achieved by assigning appropriate thermal expansion coefficient to the region of matrix being transformed into hydride [20]. Singh et al. [21] predicted the habit plane of δ-hydride in α-Zr matrix using Puls' [20] methodology by minimization of the accommodation energy with respect to orientation. Leitch and Shi [17] computed the dependence of accommodation energy of hydrides in α-Zr matrix assuming hydride precipitate of different geometries. It was observed that the accommodation energy was minimum for a partially wedge shaped and for round hydride plates [17].

It has been reported that increase in hydrogen isotope concentration in Zr–H solid solution results in increase in lattice parameters of Zr and vice-versa [22]. Thus the formation of hydride from Zr–H solid solution will result in increase in volume for the region transforming to hydride and decrease in volume for rest of the matrix, which is getting depleted of hydrogen. Since the volume of hydride free region is much larger than the volume of hydride, the expansion or contraction of the same may influence the stress field and accommodation energy. However, till now all the investigations reported in literature [17,20,21] considers the volume change associated with hydride formation with respect to zirconium and ignores the volume change in the rest of the region. In this work for the first time simultaneous simulation of hydride expansion and matrix contraction and vice-versa has been carried out. The model was partitioned in two regions, viz., a small plate shaped region which is transformed to hydride and rest of the region which is Zr–H solid solution or matrix. Appropriate thermal expansion coefficients and elasto-plastic properties were assigned to the region being transformed to hydride and Zr–H solid solution. In the Leitch and Shi's work [17], the computational results were applicable to the case of hydride nucleation and hence only matrix was assigned elasto-plastic properties. In the present work since growth (expansion) and shrinkage (contraction) was being simulated, both hydride and matrix were assigned elasto-plastic properties. The expansion of hydride was simulated by increasing the temperature of the partitioned region being transformed to hydride (resulting in increase in volume of the partitioned region) and simultaneously decreasing the temperature of the matrix (resulting in decrease in volume of the region surrounding the partitioned region). The total strain imposed is equal to the product of thermal expansion coefficient and increase in the temperature. The contraction of hydride was simulated in the present investigation by reversing the temperature change imposed in the previous step to zero for the partitioned region as well as for the matrix. In doing so, the thermal expansion coefficients of the respective regions remain unchanged but the sign of temperature change is reversed resulting in opposite strain in the respective regions.

3. Computation of stress field

The stress field of δ-hydride in α-Zr single crystal was computed by initial strain method [23]. Transformation of the zirconium hydrogen solid solution into δ-hydride is associated with about 17% increase in volume [18,19] of the region where a hydride plate appears. The close packed planes of α-Zr and δ-hydride bear an orientation relationship of $(111)_\delta \| (0001)_\alpha$ [18]. The misfit strain along the hydride plate is designated as e_{11} and the misfit strain normal to the hydride platelet is designated as e_{22} [18]. For all the computations reported in this work stress free transformation strain e_{11} and e_{22} at 25, 200 and 400 °C as shown in Fig. 2(a) were used [18,19] to simulate transformation of matrix to hydride. To simulate the depletion of hydrogen from the matrix during hydride precipitation or enhanced hydrogen solid solubility during hydride dissolution the transformation strains reported by MacEwen et al. [22] were used. The transformation strain data used in this work were for Zr–H solid solution containing 100 wppm deuterium [22] at 25, 200 and 400 °C and are shown in Fig. 2(a).

The body was partitioned into two parts, viz., hydride and matrix. The phase transformation of zirconium hydrogen solid solution to hydride was simulated by imposing an incrementally increased expansion in partitioned region called hydride, which was assigned with appropriate expansion coefficients [17,20] (Fig. 2(a)) to achieve the desired volume expansion. The effect of corresponding depletion of hydrogen from zirconium hydrogen solid solution due to hydride formation was simulated by imposing an incrementally increased contraction in the partitioned region called matrix, which was assigned with appropriate expansion coefficients and temperature change [17,20] to achieve the desired volume contraction [22] resulting from stress free transformation strains shown in Fig. 2(a). Singh et al. [21] reported that

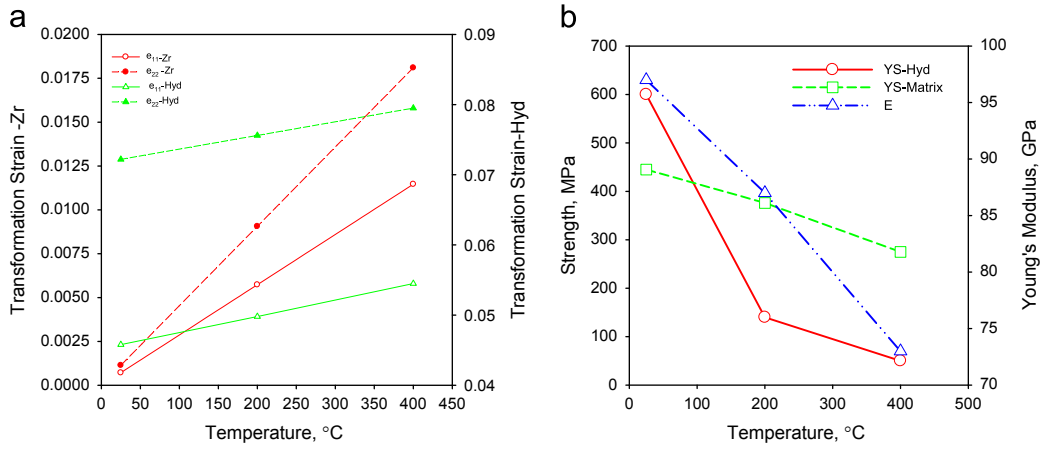

Fig. 2. Material properties of α-Zr matrix and δ-hydride used in the present investigation. (a) Transformation strains for Zr–H solid solution containing 100 wppm of hydrogen isotope and δ-hydride and (b) yield strength (YS) and Young's modulus (E) as a function of temperature.

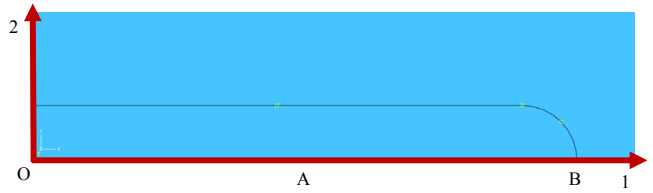

Fig. 3. The shape of hydride plate embedded in a matrix (shown partially) considered for the stress field computation is shown schematically. The variation in stress component S_{22} and hydrostatic stress along the line OAB1 is shown in Figs. 5 and 6, respectively. The computations were carried out for both fully and semi-constrained hydride. The unit of length AU is defined as 1/100 of the distance OB.

the contribution to accommodation energy of hydrides in Zirconium matrix is mainly due to orthotropic transformation strains of the hydrides with only a small contribution due to transversely isotropic elastic constants of hcp zirconium, work-hardening in hydride and zirconium, and anisotropic flow behaviour of zirconium. Hence in the present work, both matrix and hydride were modelled as linear elastic and perfectly plastic solids. Both hydride precipitate and matrix were modelled with identical Young's modulus as shown in Fig. 2(b). The Poisson's ratio of the hydride was taken as 0.333 [24] whereas that of the same for hcp Zr-matrix was taken as 0.342 [25].

The yield strength (YS) of the hydride [24] and that of the matrix [10] shown in Fig. 2(b) at 25, 200 and 400 °C were used in the computations. Both matrix and hydride were treated as isotropic elastic perfectly plastic solids using von Misses' yield criterion and the associated flow rule [17,20,24]. The ratio of the largest linear extent of the hydride to that of matrix was 20 [17,21]. The ratio of hydride plate thickness with its diameter was 0.05 [20,21]. Edge biased meshing with finer mesh near the hydride–matrix interface was considered [21]. A series of computations with decreasing mesh size ensured the values reported in this work are mesh size independent. The number of elements in the model was 8443 and the number of nodes was 25,714.

The shape of the hydride plate considered for this computation is shown schematically in Fig. 3 and the computations were carried out for plane strain (PE) and for axi-symmetric (AX) cases. The unit of length AU is chosen to be 1/100 of the distance OB. The stress field was computed in two steps. The computations of the stress field in step 1 simulated precipitation i.e. a growing hydride, where the desired expansion strains for the hydride and the contraction strain for the Zr–H solid solution up to maximum values were incrementally imposed. The computation of stress field in step 2 simulated dissolution, i.e. a contracting hydride, where the temperature change imposed in step 1 for both the partitioned regions called hydride and the matrix were incrementally reversed. It is evident from Fig. 2(b) that above 100 °C the hydride yield strength is lower than that of matrix, which may tempt one to think that the stress field of hydride may diminish with increase in temperature. However, it may be noted that the stress free transformation strains of hydrides increases with increase in temperature [19]. It is felt that because of large dilatation associated with the formation of hydrides, the nature of constraint imposed on the hydride will govern the stress field rather than the flow stress of the hydride. A hydride plate embedded inside the matrix will be fully constrained and hence a significant proportion of dilatation has to be accommodated inside the matrix resulting in stress field even for softer hydride. However, when hydride is precipitating near the surface as in the case of a hydride blister [26], a softer hydride will not result in significant stress in the matrix. In order to bring out the influence of flow stress of hydrides on temperature dependence of the stress field of hydrides in the matrix surrounding it, the stress field was computed for both fully constrained and semi-constrained cases in the present investigation. Due to the two-folded symmetry of the problem only a quarter ($x_1 \geq 0$, $x_2 \geq 0$) of the body was considered. The body was assumed to be very large compared to the size of the hydride. The part that was computed was bound by the segments $x_1 \leq R$ and $x_2 \leq R$, where R was 20 times the major dimension of the hydride. For the fully constrained case the boundary conditions were as follows:

$U_2 = 0$ along the boundary $x_2 = 0$,
$U_1 = 0$ along the boundary $x_1 = 0$.
For the semi-constrained case the boundary conditions were
$U_1 = 0$ along the boundary $x_1 = 0$.
$S_{11} = 0$ along the boundary $x_1 = 0$.
Further, for both cases
$S_{12} = 0$ along the boundary $x_1 = 0$ and the boundary $x_2 = 0$.
U_i is the displacement along ith direction. The remote boundary at $x_1 = R$ and $x_2 = R$ is traction free.

4. Results

Fig. 4 shows the contour plot of the stress component S_{22} acting normal to hydride plate (direction x_2 shown in Fig. 3). The contour plots shown in this figure pertain to the plane strain case computed using material properties at 25 °C (Fig. 4(a) and (b)) and 400 °C (Fig. 4(c) and (d)). It is evident from this figure that the

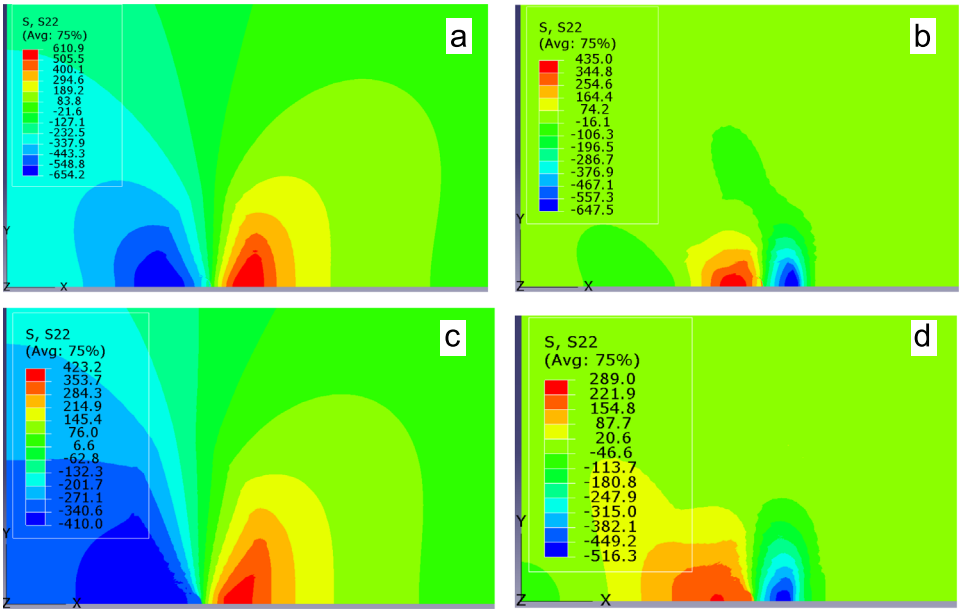

Fig. 4. Contour plots S_{22}, stress component normal to major hydride plate dimension of (a) expanding (precipitation) and (b) contracting (dissolution) hydride computed for fully constrained plane strain case using material properties at 25 °C for the hydride plate shape shown schematically in Fig. 3. The corresponding plot obtained using material properties at 400 °C for (c) expanding (precipitation) and (d) contracting (dissolution) is also shown.

S_{22} in the matrix near the tip of the hydride plate (Fig. 4(a) and (c)) for an expanding hydride is tensile whereas the same for a contracting hydride is compressive (Fig. 4(b) and (d)). The contour plots of the stress component S_{22} near the hydride–matrix interface for the axi-symmetric case was similar to that obtained for a plane strain case. Similar results were obtained for the hydrostatic stress variation in matrix surrounding the hydride plate during expansion and contraction. Fig. 5 shows the plots of S_{22} along the line OAB1 (shown in Fig. 3) parallel to direction x_1 for both (a) plane strain and (b) axi-symmetric cases using material properties at 25, 200 and 400 °C for the fully constrained case. The axis of symmetry is $x_1=0$. The values of S_{22} for expansion are shown with solid lines whereas those for contraction are shown with dashed lines. The magnitude of S_{22} in the hydride and in the matrix shown in Fig. 5 for both plane strain and axi-symmetric cases are similar for expanding as well as for contracting hydride plates. For the expanding hydride, the S_{22} component is compressive within the hydride plate, changes sign across the hydride–matrix interface and becomes tensile for the matrix near the interface. For a fully dissolved hydride plate, the S_{22} component is tensile within the pre-existing hydride plate, changes sign across the pre-existing hydride plate and matrix interface and becomes compressive in the matrix near the pre-existing hydride–matrix interface. For expanding and fully dissolved hydrides the magnitude of computed values of S_{22} in the matrix was observed to decay rapidly with increase in distance from the hydride–matrix interface.

Saint-Venant's principle allow a determination of the less complicated remote stress distribution that results from the rather complicated load exerted by the hydride [27]. This may be understood if one considers an analogy with the stress field caused by a combination of edge dislocations. A single dislocation exerts a stress field that is proportional to the inverse of the distance $(1/r)$. For a dislocation dipole with one edge at $r=-\varepsilon$ and one edge at $r=\varepsilon$ the stress is given by superposition as follows:

$$\frac{1}{r-\varepsilon}-\frac{1}{r+\varepsilon}\to\frac{2\varepsilon}{r^2}\quad\text{as}\quad\frac{r}{\varepsilon}\to\infty,$$

meaning that the stress decays in proportion to the inverse squared distance. Similarly it is found that the stress decay in proportion to the inverse cube of the distance if two counteracting dipoles are superimposed [27]. In the plane strain case the dislocation dipole form an inserted strip that replaces the hydride. The distance ε is scaling with the distance OB in Fig. 3. At large distances the stresses caused by the hydride will have the same dependence on the distance as that of the hydride. In the axi-symmetric case the suggestion is that an inserted expanding circular disk (the hydride) is viewed as two counteracting dislocation dipoles.

For the fully constrained case of hydride precipitation, the stress component normal to the major hydride plate dimension (cf. Fig. 3) is tensile stress in the matrix located near the tip of the plate and for the case of the fully dissolved hydride, the corresponding stress component is compressive. The corresponding plot of hydrostatic stress variation in fully constrained hydride and matrix is shown in Fig. 6 for (a) plane strain and (b) axi-symmetric cases. The variations in hydrostatic stress for expansion (solid lines) and contraction (dashed lines) were similar in nature to the variation in S_{22}.

It may be pointed out here that the yield strength of hydride at 400 °C is only 50 MPa which is much lower as compared to yield stress of matrix viz., 270 MPa at 400 °C. However, such a soft hydride has also exerted a stress in the matrix, which is comparable to the yield strength of the matrix in the fully constrained case. The computed hydrostatic stress variation for the semi-constrained case obtained using material properties at 25, 200 and 400 °C are shown in Fig. 7. As is evident from this figure the computed stress field in the matrix during both expansion and contraction is insignificant as compared to the fully constrained case at all temperatures. The hydrostatic stress inside hydride is 400 MPa at 25 °C when the hydride is harder than the matrix. As the temperature increased, the flow stress of the hydride decreases and the hydrostatic stress in the hydride also decreased. In the latter case the hydrostatic stress decreased to less than 100 MPa. This confirms that for a given stress free transformation strain the stress field of hydride is governed predominantly by the nature of the constraint rather than the flow stress of the hydride.

5. Discussion

It is known that presence of a brittle phase makes the host matrix brittle which manifests as the reduction in impact and

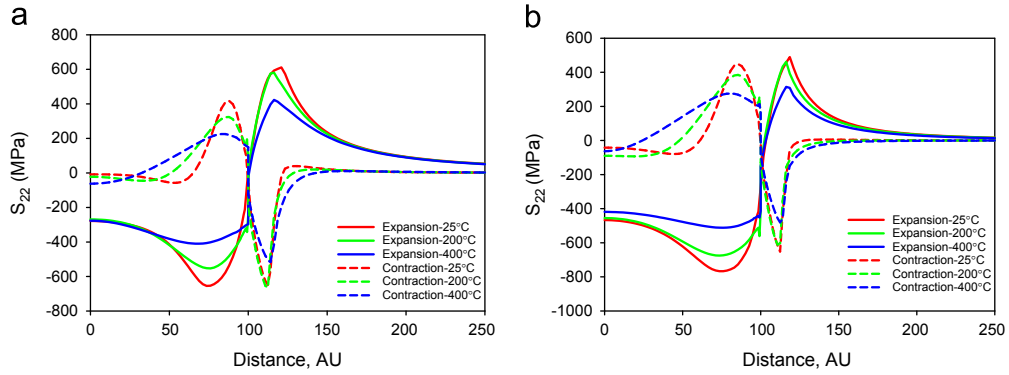

Fig. 5. Plots of S_{22} as a function of distance (Arbitrary units—AU) along a line passing though OAB1 parallel to direction 1 (Fig. 3) for both the (a) axi-symmetric and (b) plane strain fully constrained cases. The computations were made for both expanding (solid lines) and contracting (dashed lines) hydride plates using material properties at 25, 200 and 400 °C (Fig. 2).

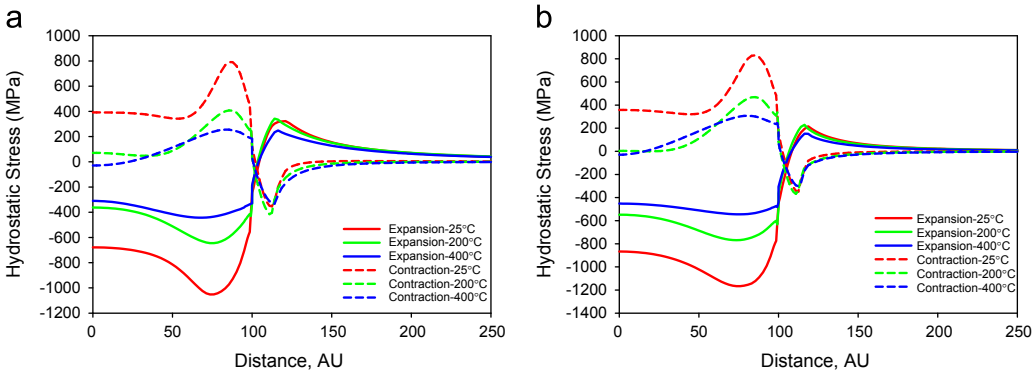

Fig. 6. Plots of hydrostatic stress as a function of distance (Arbitrary units—AU) along a line passing though OAB1 parallel to direction 1 (Fig. 3) for both the (a) axi-symmetric and (b) plane strain fully constrained cases. The computations were made for both expanding (solid lines) and contracting (dashed lines) hydride plates using material properties at 25, 200 and 400 °C (Fig. 2).

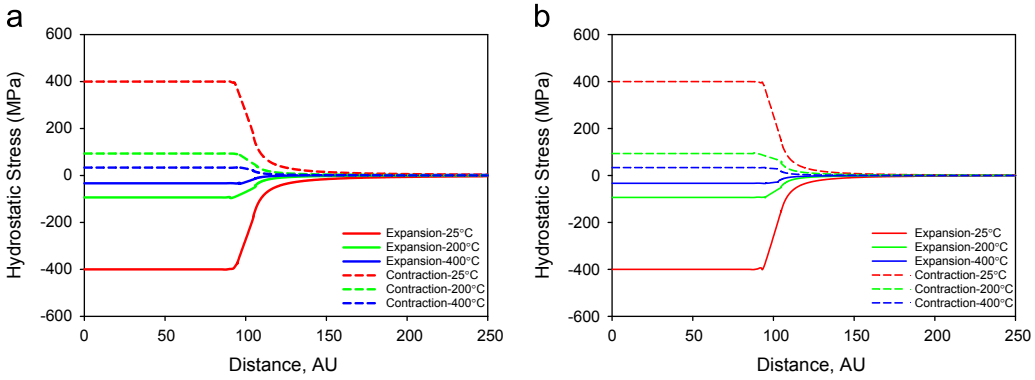

Fig. 7. Plots of hydrostatic stress as a function of distance (Arbitrary units—AU) along a line passing though OAB1 parallel to direction 1 (Fig. 3) for both the (a) axi-symmetric and (b) plane strain semi-constrained cases. The computations were made for both expanding (solid lines) and contracting (dashed lines) hydride plates using material properties at 25, 200 and 400 °C (Fig. 2).

fracture toughness. However, for significant reduction in toughness certain minimum volume fraction of embrittling phase is required. Hydrides are known to be brittle and are reported to cause embrittlement of Zr-alloys [5]. However, Zr-alloy samples containing hydrogen in the range 25–170 wppm exhibits a sharp transition from low energy fracture to high energy fracture with transition temperatures greater than 150 °C [8,9,12,16]. This type of temperature dependence of hydrided Zr-alloy has been attributed to enhanced ductility of matrix and hydrides at temperatures above 150 °C [5]. It is worth mentioning here that even the samples containing as high as 170 wppm hydrogen exhibited impact energy values comparable to unhydrided samples at 240 °C [16]. Since the test temperature of 240 °C was attained by heating up from ambient, it is expected to contain less than 30 wppm hydrogen in solution and remaining 140 wppm hydrogen as hydride [6]. Thus, at 240 °C even the presence of 140 wppm hydrogen as hydride is not causing any embrittlement in this alloy, whereas at ambient temperature just 25 wppm of hydrogen (Fig. 1 (a)) causes significant difference in impact behaviour [8].

An attempt will now be made to rationalize the influence of hydride on the temperature dependence of impact energy and fracture toughness of this material. Gross tensile ductility of Zr–2.5 Nb alloy reported by Singh et. al. [10] appears to be decreasing marginally with increase in temperature in the temperature range

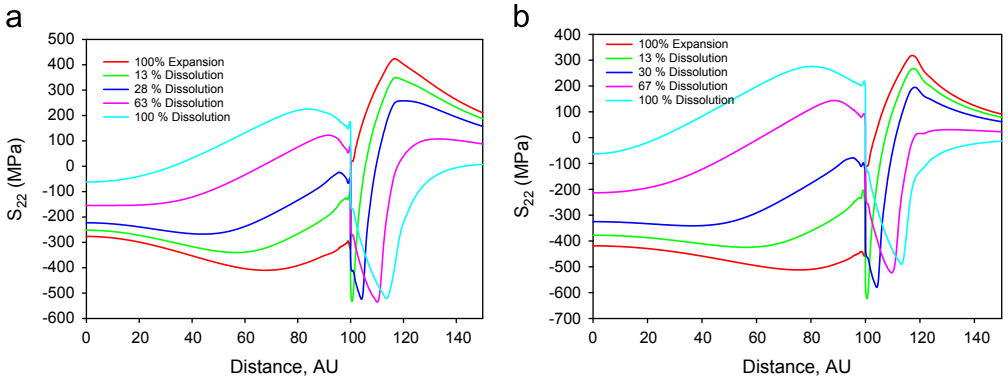

Fig. 8. Plots of S_{22} as a function of distance (Arbitrary units—AU) for partially dissolving hydride along a line passing though OAB1 parallel to direction 1 (Fig. 3) for both the (a) axi-symmetric and (b) plane strain fully constrained cases. The computations were made for different degree of hydride dissolution using material properties at 400 °C (Fig. 2).

of 25–300 °C. Puls et al. [24] had summarized the temperature dependence of yield strength of solid zirconium hydride reported in literature. Though large scatter is observed between the yield strength values of δ-$ZrH_{(1+x)}$ reported in literature, the latter was observed to decrease with increase in temperature [24]. Simpson and Cann [11] have reported fracture toughness of δ-hydride (obtained by hydriding Zr–2.5 Nb alloy) and the same was shown to be exhibiting brittle failure even at temperature up to 300 °C. Thus limited increase in tensile ductility of matrix [10] and brittle behaviour of hydride [11] in temperature range of 25–300 °C, cannot explain the sharp transition in temperature dependence of impact and fracture toughness of this material.

It is well-known that microstructure of the material governs its material properties. The microstructural parameters such as grain size, second phase volume fraction, dislocation density, and texture are reported to affect mechanical properties. However, a close look at Fig. 1(a) shows that a drastic change in impact behaviour is observed with a rise of 50 °C in temperature. Similarly, the fracture behaviour changes significantly with an increase of 100 °C in temperature. With a change of 50–100 °C in temperature none of the microstructural parameters listed above are likely to change resulting in such a significant change in impact and fracture behaviour. It is felt that the state of stress is dependent on the tendency of hydride to expand or contract and whether hydride is fully constrained or semi-constrained. The hydride plate will expand during cooling while it will contract during heating. Incidentally for both impact and fracture toughness tests the test temperatures are attained by heating the samples from ambient to the desired test temperatures. Hence as the test temperature is increased the hydrides will contract. The variation in the stress component S_{22} in the hydride and matrix surrounding it for expanding (solid lines—expansion) and contracting (dashed lines—contraction) hydride is shown in Fig. 5 for fully constrained case. The terminal solid solubility of hydrogen in Zr-alloys exhibits an Arrhenius type relationship, with solid solubility increasing with increase in temperature. Thus as the temperature is increased a pre-existing hydride plate will start dissolving partially. The plots of S_{22} for partially dissolving hydride along a line passing though OAB1 parallel to direction 1 (Fig. 3) for both the (a) plane strain and (b) axi-symmetric fully constrained cases is shown in Fig. 8. The computations were carried out for different degree of hydride dissolution using material properties at 400 °C (Fig. 2). It is evident that for a partially dissolved hydride case, the hydride is still under compressive stress, the matrix just in the vicinity of hydride–matrix interface is under very large compressive stress and the matrix beyond this region is under tensile stress. As the degree of dissolution increases the magnitude of compressive stress in the hydride decreases and the magnitude of compressive stress in the vicinity of matrix–hydride interface remain unchanged but the width of this zone became wider and the tensile stress in the matrix beyond this region decreased. The deviatoric stresses in the matrix near the hydride–matrix interface are large enough to cause plastic deformation, as a result of which the magnitude of stress remains practically constant. With further increase in the degree of deformation the region under plastic deformation becomes wider. This behaviour is similar to a crack loaded in tension in an elasto-plastic material, where increase of stress intensity factor results in increase of plastic zone size but the maximum stress remains unchanged. The plots of S_{22} obtained using material properties at 25 and 200 °C were similar. Thus both a partially dissolved hydride and matrix under compressive stress will imply that embrittlement effect of hydride is lost as it starts dissolving in the matrix, which is a key result of this investigation.

The externally applied stress will get modified due to the stress field of hydride. A tensile stress component (Fig. 5) existing in the matrix near the hydride–matrix interface during expansion will facilitate crack growth through the matrix while the compressive stress component (Fig. 8) in the matrix near the hydride–matrix interface during contraction will make crack growth through the matrix difficult. Thus the stress field of partially dissolving (contracting) hydride may probably be responsible for the restoration of toughness of this alloy above 150 °C.

It will be interesting to evaluate the influence of hydride on toughness of this alloy by approaching the test temperature from a peak temperature during cooling. Though to the best of our knowledge no such results have been reported, during delayed hydride cracking (DHC) tests [28,29], the test temperature is attained by cooling from a peak temperature. During DHC test crack growth does occur through hydride–matrix composite at least up to a temperature of 283 °C, thereby suggesting that this alloy is susceptible to HE at temperatures between 150 and 283 °C when test temperature is attained by cooling from a peak temperature.

6. Conclusions

A Finite element method was used to compute the stress field for expanding (precipitation) and contracting (dissolution) hydride for fully constrained and semi-constrained cases using material property of hydride and matrix at 25, 200 and 400 °C. Simultaneous hydride expansion and matrix contraction and vice-versa were carried out in order to simulate hydride precipitation and dissolution, respectively. It was observed that the stress field is predominantly governed by the nature of constraint on hydride rather that the flow stresses of hydride. The stress component in

the matrix acting normal to a hydride plate near the hydride–matrix interface during expansion was tensile while the same for a partially dissolving hydride was compressive for the fully constrained case not only at 25 °C where hydride is harder than matrix but also at 200 and 400 °C where hydride is much softer than matrix. The compressive stress field of a partially contracting hydride plate will modify the externally applied stress and may prevent the crack growth through matrix and thereby enhancing the resistance to hydride embrittlement of this alloy above 150 °C when test temperature is approached by heating from a lower temperature.

Acknowledgement

Constant encouragement and invaluable support provided by Dr. R.K. Sinha and Dr. S. Banerjee, respectively, present and former Chairman, Atomic Energy Commission and Secretary, Department of Atomic Energy, Government of India and Dr. A.K. Suri, Director, Materials Group, BARC, Mumbai is acknowledged. Dr. Singh's association with Malmö University as a Marie Curie Incoming International fellow was financially supported by the European Commission under its FP6 programme to promote researchers mobility into European Union (Contract nos. MIF1-CT-2005-006844 and MIF2-CT-2006-980016).

References

[1] W. Dietz, Structural materials, in: R.W. Cahn, P. Haasen, E.J. Kramer, (Eds.), Materials Science and Technology: A Comprehensive Treatment, 10B Nuclear Materials, Chapter 8 (1994) p. 53.
[2] C. Lemaignan, A.T. Motta, Structural materials, in: R.W. Cahn, P. Haasen, E.J. Kramer, (Eds.), Materials Science and Technology: A Comprehensive Treatment, 10B Nuclear Materials, Chapter 7, (1994) p.1.
[3] C.E. Coleman, B.A. Cheadle, C.D. Cann, J.R. Theaker, Development of pressure tubes with service life greater than 30 years, in: Zr in the Nuclear Industry: 11th International Symposium, E.R. Bradley, G.P. Sabol (Eds.), ASTM STP, vol. 1295 (1996) p. 884.
[4] M.B. Elmoselhi, B.D. Warr, S. McIntyre, A study of hydrogen uptake mechanism in zirconium alloys, in: Zr in the Nuclear Industry: 10th International Symposium, A.M. Garde, E.R. Bradley (Eds.), ASTM STP, vol. 1245 (1994) p. 62.
[5] D.O. Northwood, U. Kosasih, Intl. Met. Rev. 28 (2) (1983) 92.
[6] R.N. Singh, S. Mukherjee, AnujaGupta, S. Banerjee, J. Alloys Compd. 389 (2005) 102.
[7] Z.L. Pan, I.G. Ritchie, M.P. Puls, J. Nucl. Mater. 228 (2) (1996) 227.
[8] R.N. Singh, U.K. Viswanathan, P.M. Sunil Kumar, S. Satheesh, Per Stahle Anantharaman, Eng. Des. 241 (2011) 2425–2436.
[9] R.N. Singh, P. Ståhle, N.S. Srinivasan, Influence of hydrogen content on axial fracture toughness parameters of Zr–2.5 Nb pressure tube alloy in the temperature range of 306–573 K, in: Proceedings of ICAPP'06, Reno, NV, USA, June 4–8, 2006, Paper 6138.
[10] R.N. Singh, S. Mukherjee, R. Kishore, B.P. Kashyap, J. Nucl. Mater. 345 (2005) 146.
[11] L.A. Simpson, C.D. Cann, J. Nucl. Mater. 87 (1979) 303.
[12] P.H. Davies, C.P. Sterns, Fracture toughness testing of zircaloy-2 pressure tube material with radial hydrides using direct-current potential drop, in: J.H. Underwood, R. Chait, C.W. Smith, D.P. Wilhem, W.A. Andrews, J.C. Newman (Eds.), ASTM STP, vol. 905 (1986) p. 379.
[13] F.H. Huang, Fracture toughness evaluation for zircaloy-2 pressure tubes with the electric-potential method, in: Proceedings of ASTM International Symposium on Small Specimen Test Techniques Applied to Nuclear Reactor Vessel Thermal Annealing and Plant Life Extension, New Orlearns, LA, USA, 29–31 January, 1992, pp. 182–198.
[14] S.I. Honda, Nucl. Eng. Des. 81 (1984) 159.
[15] L.A. Simpson, Metall. Trans. 12A (1981) 2113.
[16] U.K. Viswanathan, R.N. Singh, C.B. Basak, S. Anantharaman, K.C. Sahoo, J. Nucl. Mater. 350 (2006) 310.
[17] B.W. Leitch, S.-Q. Shi, Modelling Simul. Mater. Sci. Eng. 4 (1996) 281.
[18] G.J.C. Carpenter, J. Nucl. Mater. 48 (1973) 264.
[19] R.N. Singh, P. Ståhle, A.R. Massih, A.A. Shmakov, J. Alloys Compd. 436 (2007) 150–154.
[20] B.W. Leitch, M.P. Puls, Metall. Trans. 23A (1992) 797.
[21] R.N. Singh, P. Ståhle, Leslie Banks-Sills, Matti Ristmanaa, S. Banerjee, Defect Diffusion Forum 279 (2008) 105.
[22] S.R. MacEwen, C.E. Coleman, C.E. Ells, Acta Metall. 33 (1985) 753.
[23] S. Sen, R. Balasubramaniam, R. Sethuraman, Acta Mater. 44 (1996) 437.
[24] M.P. Puls, J. San-Qiang Shi, J. Nucl. Mater. 336 (2005) 73.
[25] D.O. Northwood, I.M. London, L.E. Bahen, J. Nucl. Mater. 55 (1975) 299.
[26] R.N. Singh, P. Ståhle, K. Sairam, J.K. Chakravartty, B.P. Kashyap, Stress-field computation for hydride blister forming in zr-alloys, in: Proceedings of the Water Reactor Fuel Performance Meeting—WRFPM 2008, Seoul, South Korea, 19–23, October 2008, Paper no. 8137.
[27] Y.C. Fung, Foundations of Solid Mechanics, Prentice-Hall, Engle Wood Cliffs, NJ, USA, 1965.
[28] S. Sagat, C.K. Chow, M.P. Puls, C.E. Coleman, J. Nucl. Mater. 279 (2000) 107.
[29] R.N. Singh, P. Ståhle, J.K. Chakravartty, A.A. Shmakov, Mater. Sci. Eng.: A 523 (2009) 112.